

# Discrete Scale Invariance in the Cascade Heart Rate Variability of Healthy Humans

D.C. Lin

Mechanical and Industrial Engineering Department  
Ryerson University, Toronto, Ontario, M5B 2K3

November 10, 2018

## Abstract

Evidence of discrete scale invariance (DSI) in daytime healthy heart rate variability (HRV) is presented based on the log-periodic power law scaling of the heart beat interval increment. Our analysis suggests multiple DSI groups and a dynamic cascading process. A cascade model is presented to simulate such a property.

## 1 Introduction

The phenomenon of heart rate variability (HRV) in humans describes the beat-to-beat, apparently random, fluctuation of the heart rate<sup>1</sup>. HRV measured by the time span between ventricular contractions, known as the beat-to-beat RR interval (RRi), is also known to share many characteristics found in other natural phenomena. For example, daytime RRi in healthy humans exhibits 1/f-like power spectrum<sup>2</sup>, multifractal scaling<sup>3,4</sup>, and similar increment distribution observed in fluid turbulence<sup>4</sup>. These characteristics may vary significantly in heart disease patients depending on the severity of the disease<sup>1,5</sup>.

The origin and the generation of HRV remain the biggest challenges in the contemporary HRV research. Although the respiratory and vascular systems constantly modulate the heart rate, they do not explain the large percentage of

the broad-band (multifractal) signal power in HRV. For example, it is unlikely that this broad-band feature results directly from the output of the narrow-band respiratory dynamics<sup>6</sup>. Also, it is known that the level and the variability of blood pressure and heart rate can change significantly from upright to supine positions. In a 42-day long bed rest test, Fortrat et al. showed that the variation in blood pressure and heart before and after the test are qualitatively different, suggesting separate control mechanisms for generating their variability<sup>7</sup>. It is thus believed that a more sophisticated structure may exist, which integrates the feedback from receptors to create the pattern of HRV<sup>8</sup>.

Apart from its origin, some progress on the HRV generating mechanism may be possible by using the discrete (lattice) multiplicative cascade model<sup>4</sup>. This is purely a phenomenology approach that does not prescribe to any physiology term. Nonetheless, encouraging results were obtained that are consistent with the physiological data in health and in certain heart disease<sup>4</sup>. The main purpose of this work is to investigate the basis of this modeling strategy. Our approach is based on the scale invariant symmetry implied from the HRV phenomenology<sup>4,9,10</sup>. Since RRI cannot be defined between heart beats, it is appropriate to consider discrete scale invariance (DSI) in HRV. It is known that discrete cascade implies DSI<sup>11~15</sup>. Better characterization of DSI in HRV is thus important since it is the necessary condition for the multifractal scaling observed in HRV. The existence of cascade is also significant because it represents a very different approach of the cardiovascular dynamical system from feedback control that is additive in principle. The idea will support the previous studies that a direct influence from baroreflex to multifractal HRV is unlikely<sup>7</sup>, as well as the need to search for a role by the higher control centers in HRV<sup>8</sup>.

The consequence of DSI is an oscillating scaling law with a well-defined power law period. Such a scaling law is said to exhibit log-periodicity (LP). In this work, we analyzed DSI in daytime healthy HRV by searching LP in

the scaling of HRV. Typically, LP is “averaged out” in the process of finding the scaling law. Using the technique called “rephasing,” this problem can be effectively resolved and evidence of multiple DSI groups in the healthy daytime RRi data was found. In light of this new result, a cascade model is constructed using random branching law to reproduce not only some of the known HRV phenomenology, but also the multiple DSI characteristics.

The results of this work are organized in five sections. In Section 2, a brief review of the notion of DSI is given. The numerical procedures for identifying the DSI property from time series are described in Section 3. Numerical examples and results on daytime heart rate data sets are given in Section 4. Concluding remarks are given in the last Section.

## 2 Discrete Scale Invariance and Rephasing

### 2.1 Ideas of Discrete Scale Invariance in Physical Systems

A random processes  $x(t)$  is said to possess continuous scale invariant symmetry<sup>13</sup> if its distribution is preserved after the change of variables,  $t \rightarrow \lambda t$ ,  $x \rightarrow x/\mu$  where  $\lambda$  and  $\mu(\lambda)$  are real numbers; i.e.,

$$x(t) = \frac{1}{\mu}x(\lambda t). \quad (1)$$

DSI is defined when (1) only holds for a countable set of scale factors  $\lambda_1, \lambda_2, \dots$ . Scale invariance implies power law. The power law in DSI has a log-periodic correction of frequency  $1/\log(\lambda)$ : i.e.,  $x(t) = t^\gamma F(\log(t)/\log(\lambda))$  where  $\gamma = \log \mu / \log \lambda$  and  $F(x) = F(x+1)$ . Generally<sup>15</sup>, one can consider  $x(t) = C_t t^{\gamma'}$ ,  $C_t$  being  $t$ -dependent, and  $\gamma' = \gamma + 2\pi ni / \log(\lambda)$  is a complex number for  $n = 1, 2, \dots$ . Novikov suggested LP in the small scale energy cascade of the turbulent flow<sup>14</sup>. Sornette and co-workers showed that LP exists more generally in physical and financial systems, such as turbulence<sup>15</sup>, earthquake<sup>16</sup>, rupture<sup>17</sup> and stock market crashes<sup>18</sup>.

The existence of the discrete scale factor implies a hierarchical structure. This link can be simply illustrated by the middle third Cantor set with the scale factor  $\lambda = 3$ . With proper rescaling, a precise copy of the set is only obtained with a 3-fold magnification of the scale<sup>13</sup>. If  $x(t)$  denotes the Lebesgue measure at scale  $t$ , the Cantor set can be modeled by (1) using  $\lambda = 3$  and  $\mu = \lambda^{-\log(2)/\log(3)}$ . Thus, the power law exponent of  $x(t)$  (the box dimension of the Cantor set<sup>19</sup>) assumes a log-periodic oscillation of frequency  $1/\log(3)$  about its mean value  $\log(2)/\log(3)$ .

The hierarchical structure can be a dynamic object as a result of some time-dependent branching law. Such a dynamic hierarchy is believed to exist, for example, in the cascade paradigm of the energy exchange in fluid turbulence where the break-down or “branching” of large-scale vortices into ones of smaller scales can occur randomly in space-time with the energy re-distribution following a multiplication scheme. In data analysis, the dynamic hierarchy poses a technical difficulty for finding the scale factor  $\lambda$  since LP may be averaged out in the process of obtaining the power law. Zhou and Sornette proposed to conduct averaging *after* rephasing or re-aligning data segments using a central maximum criterion<sup>15</sup>. Using this technique, these authors successfully extracted LP in turbulence and proposed the DSI symmetry and cascade. The rephasing technique is adopted in this work. Instead of the central maximum criterion, the cross-correlation property of the data segments will be used (see step (d) below).

## 2.2 Rephasing RRI Data

Let  $\mathbf{r}(t)$  denote the RRI between the  $t^{\text{th}}$  and  $(t + 1)^{\text{th}}$  heart beats. Based on the turbulence analogy of HRV<sup>4</sup>, we focus on the LP in the scaling exponent of the empirical law  $\mathcal{S}(\tau, p) = \langle |\Delta\mathbf{r}(\tau)|^p \rangle \sim \tau^{\zeta(\tau, p)}$  where  $\Delta\mathbf{r}(\tau) = \mathbf{r}(t + \tau) - \mathbf{r}(t)$  and  $p$  is a real number. The implementation of the rephasing follows a 8-step

algorithm; see Fig. 1.

- (a) Divide  $\mathbf{r}(t)$  into  $M$  nonoverlapping segments  $\{\mathcal{R}_1, \dots, \mathcal{R}_M\}$ .
- (b) For  $\mathbf{r}(t) \in \mathcal{R}_i$ , calculate  $\mathcal{S}_i(\tau, p) = \langle |\Delta \mathbf{r}(\tau)|^p \rangle$ .
- (c) Apply a low-pass  $(K, L)$  Savitzky-Golay (SG) filter<sup>8</sup> to  $\mathcal{S}_i(\tau, p)$  and calculate its first derivative to obtain a  $\tau$ -dependent  $\zeta_i(\tau, p)$  for  $i = 1, \dots, M$ . The  $(K, L)$  SG filter performs a  $K^{\text{th}}$  order polynomial fit over  $L$  samples<sup>15</sup>. It can produce a smoothing effect in the high frequency while preserving the statistical moments of the signal up to the order of the filter.
- (d) Randomly select the  $i$ th segment as the base segment and compute the cross-correlation  $C_{i,j}^{K,L}(\kappa)$  between  $\zeta_i(\tau, p)$  and  $\zeta_j(\tau + \kappa, p)$  for  $j \neq i$ .
- (e) Shift the time origin of  $\zeta_j(\tau, p)$  by  $\Delta_j$ , where  $\max(C_{i,j}^{K,L}) = C_{i,j}^{K,L}(-\Delta_j)$ , so that the cross-correlation between  $\zeta_i(\tau, p)$  and the shifted  $\zeta_j(\Delta_j + \tau, p)$  has a maximum at zero time lag. Note that  $\Delta_i = 0$  for the base segment.
- (f) Average the shifted  $\zeta_j(\tau + \Delta_j, p)$ ,  $j = 1, \dots, M$ , to obtain  $Z_{K,L}(\tau, p)$ .
- (g) Compute the spectrum of  $Z_{K,L}(\tau, p)$ .
- (h) Return to (c) with different  $K, L$  values.

A Lomb periodogram<sup>20</sup>  $\mathcal{L}(f)$  is used to estimate the spectrum of  $Z_{K,L}(\tau, p)$  for its superiority in handling situations where noise plays a fundamental role in the signal, as well as its capability in handling small data set.

Although the above algorithm provides the systematic steps to estimate the log-periodic component, noise in the empirical data can also generate spurious peaks in the Lomb periodogram. For independent Gaussian noise process, this problem can be analyzed by the false alarm probability<sup>20,21</sup>:

$$P_G(f) = 1 - (1 - \exp(-\mathcal{L}(f)))^m \quad (2)$$

where  $m$  is proportional to the number of points in the spectrum. The smaller the value  $P_G(f)$  is, the more likely a genuine log-periodic component exists in

the signal. Thus, a Lomb peak with large  $P_G(f)$  suggests a chance event. Zhou and Sornette conducted extensive simulations and showed that (2) is in fact an upper bound for a number of correlated noise except for those showing long-term *persistent* correlation<sup>21</sup>. The fractional Brownian motion (fBm) of a Hurst exponent greater than 0.5 is an example where (2) does not apply. The multiple scaling exponents in healthy daytime HRV have been found to lie below such a threshold<sup>1,3,4,9</sup> and we will continue to use (2) in this work.

As shown above, DSI is characterized by the frequency  $1/\log(\lambda)$  of the LP. However, significant Lomb peaks may only capture the higher harmonics  $k/\log(\lambda)$ ,  $k \neq 1$ . It is therefore necessary to define the relation of the significant peaks. We propose a simple procedure to achieve this. First, we collect the significant peaks satisfying  $P_G \leq P_G^*$  for  $P_G^* \ll 1$  and for different SG filter parameters. Second, we form a significant Lomb peak histogram (SLPH) and locate its local maxima. These maxima identifies the most probable frequencies of the log-periodic oscillation of the power law. Let such maxima be  $f_1, \dots, f_n$ . The last step of the procedure is to search the smallest  $\lambda$  to minimize

$$d_\lambda = \sum_i^n |f_i - k_i/\log(\lambda)| \quad (3)$$

for integers  $k_i$ 's. We seek the smallest  $\lambda$  since, with finite precision in numerical computing,  $d_\lambda$  can be made arbitrarily small as  $\lambda \gg 1$ . This minimization step is simple, easy to implement and, as we show below using synthetic data, it is also effective.

### 3 Numerical Results

#### 3.1 DSI in Discrete Bounded Cascade

The rephasing algorithm introduced above was first tested on synthetic data generated by the discrete cascade<sup>4</sup>

$$x_J(t) = \Pi_j^J \omega_j(t) \quad (4)$$

where the cascade components  $\omega_j(t)$  are discrete-time processes given by

$$\omega_j(t) = 1 + \sigma_j \mathbf{w} \quad (5)$$

for  $t_k^{(j)} \leq t < t_{k+1}^{(j)}$ ,  $k = 1, 2, \dots, j = 1, \dots, J$ , and  $\mathbf{w}$  is a zero-mean Gaussian random variable of variance 1. Let  $t_{k+1}^{(j)} - t_k^{(j)} = \delta_j$ . The scale factor  $\lambda$  in the DSI hierarchy is related to  $t_k^{(j)}$ 's by

$$\delta_j / \delta_{j+1} = \lambda. \quad (6)$$

To model the bounded RRi, we further assume  $\sigma_j > \sigma_{j+1}$  to assure boundedness. This model has been used in the past to simulate HRV phenomenology, including transition of RRi increment probability density function and multi-fractal scaling<sup>4</sup>.

According to (4), we generated 30 sets of dyadic ( $\lambda = 2$ ) and triadic ( $\lambda = 3$ )  $x_J(t)$  with the corresponding  $\log(\sigma_j) = (-1.6 - 0.126j) \log(2)$  and  $\log(\sigma_j) = (-1.9 - 0.093j) \log(3)$ , respectively. Each  $x_J(t)$  has 8192 points and is divided into segments of 1024 points. Twenty-four sets of  $(K, L)$  SG filter are defined based on  $K = 3, 4, \dots, 7$ ,  $L = 7, 9, \dots, 15$ . For each combination of  $K, L$ , steps (c) to (h) in the rephasing algorithm is repeated six times based on six different base segments selected in step (d) of the algorithm. This is implemented to avoid bias from a particular segment. Significant Lomb peaks are collected based on the false alarm probability  $P_G^* < 1\%$  or  $\mathcal{L}(f) \geq 10$  and  $m = 256$  points of the Lomb periodogram. The results for  $p = 2$  is reported as no quantitative difference exists for  $p \leq 3$ . Numerical results for  $p > 3$  show more variability due to poor statistics.

FIG. 2a shows the  $\zeta_i(\tau, p)$  of a particular segment of one of the dyadic  $x_J(t)$ 's. The log-periodic oscillation with a log-period  $\log(2)$  is clearly seen. The Lomb periodogram of  $Z_{K,L}(\tau, p)$  (step (f) above) is shown in FIG. 2b based on a particular choice of  $K, L$  and the dominant LP is seen to pick up the second

harmonics of  $1/\log(2)$ . The SLPH estimated for different SG filters over 30 sets of  $x_J(t)$  is obtained in FIG. 3. The clustering of the local maxima at integer multiples of  $1/\log(2)$  is evident. The minimization (3) identifies the correct scale factor  $\lambda = 2$  for the dyadic cascade. Similar results of the tradic cascade are also found (FIG. 3). These examples demonstrate the effectiveness of the proposed numerical procedures.

### 3.2 DSI in Daytime Healthy HRV

For HRV, two databases are considered. The first set (DB1) consists of 10 ambulatory RRi recordings from healthy young adults<sup>4</sup>. These test subjects were allowed to conduct normal daily activities. The second set (DB2), available from the public domain<sup>22</sup>, consists of 18 ambulatory RRi recordings showing normal sinus rhythm. The parameters used in the numerical analysis are the same as above except the data segment length has increased to 2048 points. The choice of the segment length is a balance of two factors: small segment length results in more segments but poorer statistics in the estimation of  $\zeta_i(\tau, p)$ ; large segment length results in less segments but better estimate of  $\zeta_i(\tau, p)$ . We tried 1024 points per segment and found similar results; i.e., the group averaged  $\lambda$  value is similar to the ones reported in FIG. 5 below.

The SLPH in all cases shows well positioned local maxima that can be easily related to the harmonics of some fundamental frequency (FIG. 4). The  $\lambda$  values for DB1 and DB2 are summarized in FIG. 5. It is observed that (a) there are non-integer scale factor  $\lambda$  and (b) the  $\lambda$ 's cluster in the range of [3.5, 5.5] and the group averaged  $\lambda$  are  $\sim 4.8$  and  $\sim 4.4$  for DB1 and DB2, respectively. The noninteger  $\lambda$  unambiguously excludes the possibility of discrete cascades with one scale factor. It implies more complicated branching law and multiple DSI groups in healthy HRV.

Although HRV and turbulence exhibit similar phenomenology<sup>4</sup>, it is inter-

esting to point out the rather large  $\lambda$  value ( $> 4$ ) compared with the  $\lambda \sim 2$  in fluid turbulence<sup>10</sup>. From the discrete cascade viewpoint, a larger  $\lambda$  is compatible with the “patchiness” appearance commonly observed in the RRI of healthy humans<sup>1,3,4,9,10</sup> since the  $\omega_j(t)$ ’s of the cascade will fluctuate on a longer time scale to create the effect.

To model the multiple DSI in cascade HRV, the scale factor  $\lambda$  used in (5) is set to be a random number so that the log-periodic oscillation of  $\zeta(p)$  can vary over a range of frequencies. We generated 30 sets of  $x_J(t)$  according to (4) using uniformly distributed  $\lambda$  in the interval [2,6]. The simulated  $x_J(t)$  exhibits the “patchiness” pattern observed in the RRI data (FIG. 6), and similar scaling characteristics found in the past<sup>4</sup> (FIGs. 7a ~ 7c). The scaling exponent  $\zeta(\tau, p)$  of the power law  $\langle |\Delta x_J(\tau)|^p \rangle \sim \tau^{\zeta(\tau, p)}$  exhibits log-periodic oscillation that is captured by the well positioned local maxima in SLPH (FIGs. 7d, 7e). In addition, the average of the  $\lambda$ ’s lies close to the group-averaged  $\lambda$  values of DB1 and DB2 (FIG. 5).

## 4 Conclusion

It is known that discrete cascade leads to DSI and characterized by log-periodic modulation of the scaling property<sup>11,12</sup>. Hence, the LP reported in this work supports the view of a cascade for the multifractal generation in HRV. It implies a more sophisticated process than reflex-based control mechanisms that function on the additive basis. It also suggests the need to search for a role by the higher control centers in HRV<sup>8</sup>. It is conjectured that the cascade describes the process which integrates the regulatory feedbacks in the cardiovascular system to create the pattern of HRV.

The non-integer scale factor implies multiple DSI. This property was also reported in the screening competition of the growth of diffusion limited aggre-

gation model<sup>23,24</sup>. To the best of our knowledge, this is the first instance of multiple DSI being reported in HRV. We do not have the better knowledge of its origin, except to believe it reflects the multiple time-scale control mechanisms in the cardiovascular dynamical system.

It is tempting to search for the physiological correlate of the cascade, for example, the role of the cascade components  $\omega_j(t)$ . Based on the spectral analysis, we suggested that the large time scale components ( $\omega_j, j \sim 1$ ) capture mainly the sympatho-vagal interaction and the small time scale components ( $\omega_j, j \gg 1$ ) capture the parasympathetic activity<sup>4</sup>. However, we should caution that cascade is a modeling tool derived from statistical physics. The  $\omega_j(t)$  can therefore represent the range of micro- to macroscopic processes in the cardiovascular dynamical system.

A rather narrow range of the scale factor  $\lambda \in [3.5, 5.5]$  estimated from the two different databases implies a “stable” hierarchical structure of the cascade that does not vary sensitively with the details of the healthy population. The analysis of the identified DSI characteristics in other physiological conditions is currently underway and its result will be reported in the near future.

### **Acknowledgment**

This research is supported by Natural Science and Engineering Research Council of Canada. The author would like to thank many years of valuable comments and suggestions by Dr. R.L. Hughson of the University of Waterloo and critical comments by the anonymous referee.

## Reference

- [1] Task Force of the ESC and NASPE, *Euro. Heart J.*, **17**, 354 (1996).
- [2] M. Kobayashi and T. Musha, *IEEE Trans. Biomed. Eng.*, **29**, 456 (1982).
- [3] P.CH. Ivanov, et al., *Lett. to Nature*, **399**, 461 (1999).
- [4] D.C. Lin and R.L. Hughson, *Phys. Rev. Lett.*, **86**, 1650 (2001); D.C. Lin and R.L. Hughson, *IEEE Trans. Biomed. Engng.*, **49**, 97 (2002); D.C. Lin, *Fractals*, **11**, 63 (2003); D.C. Lin, *Phys. Rev. E*, **67**, 031914 (2003).
- [5] G.C. Butler et al., *Clin. Sci.*, **92**, 543 (1997).
- [6] Y. Yamamoto et al., *Am J. Physiol*, **269**, H480 (1995); G.C. Butler et al., *Am J Physiol*, **26**, R26 (1994).
- [7] J.O. Fortrat et al., *Auton. Neurosci.*, **86**, 192 (2001).
- [8] F. Togo and Y. Yamamoto, *Am. J. Physiol. Heart Circ. Physiol.*, **28**, H17 (2001).
- [9] H.E. Stanley, et al., *Physica A*, **281**, 60 (2000); P.Ch. Ivanov, et al., *Chaos*, **11**, 641 (2001).
- [10] P. Bernaola-Galvan, et al., *Phys. Rev. Lett.*, **87**, 168105 (2001).
- [11] F. Schmitt and D. Marsan, *Eur. Phys. J. B*, **20**, 3-6 (2001).
- [12] E. Bacry, J. Delour, and J.F. Muzy, *Phys. Rev. E*, **64**, 026103 (2001).
- [13] D. Sornette, Critical Phenomenon in Natural Sciences, Series in Synergetics, *Springer Verlag*, Heidelberg (2000).
- [14] E.A. Novikov, *Dokl. Akad. Nauk SSSR*, **168**, 1279 (1966).
- [15] W-X. Zhou and D. Sornette, *Physica D*, **165**, 94 (2002); D. Sornette, *Phys Rep*, **297**, 239 (1998).
- [16] A. Johansen, et al., *J. Geophys. Res.*, **105**, 28111 (2000); Y. Huang, et al., *J. Geophys. Res.*, **105**, 28111 (2000).
- [17] Y. Huang, et al. *Phys. Rev. E*, **55**, 6433 (1997).
- [18] A. Johansen and D. Sornette, O. Ledoit, *J. Risk*, **1**, 5 (1999).

- [19] K. Falconer, Fractal Geometry, Mathematical Foundation and Applications, *John Wiley & Sons*, Chichester (1990).
- [20] J.D. Scargle, *Astrophys. J.*, **263**, 835 (1982).
- [21] W-X. Zhou and D. Sornette, *Int. J. Mod. Phys. C*, **13**, 137 (2002).
- [22] A.L. Goldberger, et al., *Circulation*, **101**, e215 (2000).
- [23] A. Arneodo, et al., *Phys. Rev. Lett*, **68**, 3456 (1992).
- [24] D. Sornette, et al., *Phys. Rev. Lett*, **76**, 251 (1996).

## Figure Captions

FIG. 1 Sketch of the numerical procedure for rephasing. The second segment is illustrated as the base segment and rephasing was shown for  $\zeta_1(\tau + \Delta_1, p), \dots, \zeta_M(\tau + \Delta_M, p)$  ( $\Delta_j$  is determined at the maximum of the cross-correlation function between the  $j$ th and the base segments). Log-periodicity in  $Z_{K,L}(\tau, p)$  is estimated from the Lomb periodogram.

FIG. 2 (a)  $\zeta_i(\tau, p) - \langle \zeta_i(\tau, p) \rangle$  versus  $\log(\tau)$  taken from the synthetic dyadic bounded cascade. The solid line is a pure sine wave with a period of  $\log(2) \sim 0.693$ . (b) Typical Lomb periodogram of  $Z_{K,L}(\tau, 2)$  (averaged over all  $\zeta_i(\tau, p)$ 's).

FIG. 3 SLPH estimated from 30 sets of (a) synthetic dyadic bounded cascade  $x_J(t)$  and (b) triadic  $x_J(t)$ . The grid lines in (a) and (b) are drawn according to  $k/\log(2)$  and  $k/\log(3)$ ,  $k = 1, 2, \dots$ , respectively.

FIG. 4 (a) SLPH of a typical data set from DB1. The local maxima  $f_{\max}$  are marked by “+”. (b)  $f_{\max}$  versus  $k/\log(4.5)$ ,  $k = 1, 2, \dots$ , showing as the harmonics generated by the fundamental frequency  $1/\log(4.5)$ . The straight line has the slope  $1/\log(4.5)$ . (c) Similar to (a) based on a data set taken from DB2. (d) Similar to (b) based on the local maxima of (c). The straight line has the slope  $1/\log(3.1)$ . Note the local maximum between  $7/\log(3.1)$  and  $8/\log(3.1)$  was not fitted by the harmonics of  $1/\log(3.1)$ .

FIG. 5 Scale factor  $\lambda$ 's for 10 subjects in DB1, 18 subjects in DB2 and 30 sets of synthetic data  $x_J(t)$  generated by the cascade model. The group averaged  $\lambda$  values and standard deviations are superimposed and drawn as “●” and vertical bar, respectively.

FIG. 6 A typical sample of  $x_J(t)$  (top) and the RRi data (bottom) taken from

DB2. Both time series show the characteristic of “patchiness” in their fluctuation pattern.

FIG. 7 (a) to (c) show the  $1/f$ -like power spectrum, power law,  $\mathcal{S}(\tau, p)$  and the nonlinear  $\zeta(p)$  of  $\mathcal{S}(\tau, p)$ , respectively, of the  $x_J(t)$  shown in FIG. 5; see Ref. 4 for the similar characteristics reported for RRi data in healthy humans. (d) and (e) show the SLPH of two typical  $x_J(t)$ . Well-positioned local maxima in (d) and (e) capture the harmonics generated by  $\lambda$ :  $\sim 4.4$  and  $\sim 3.85$ , respectively.

This figure "fig1\_algorithm.jpg" is available in "jpg" format from:

<http://arxiv.org/ps/physics/0411039v1>

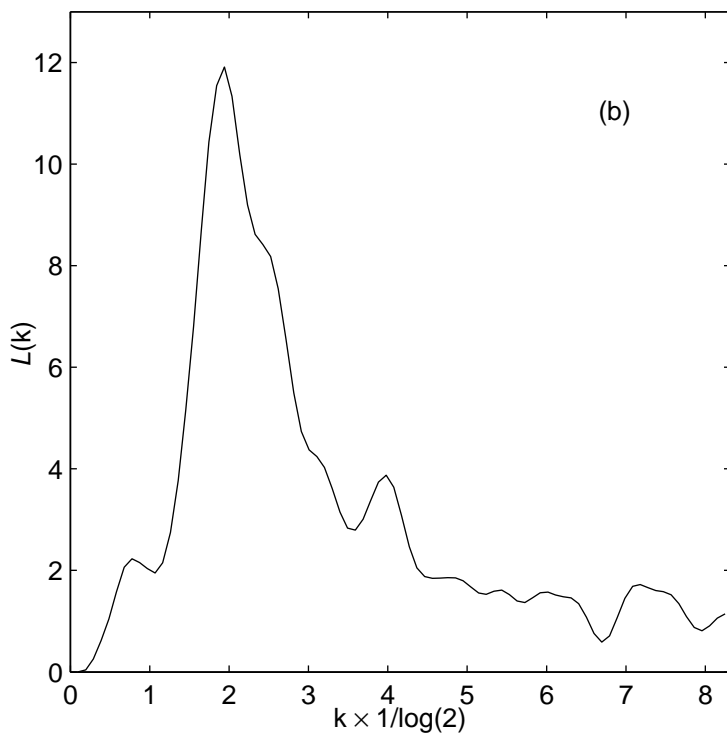
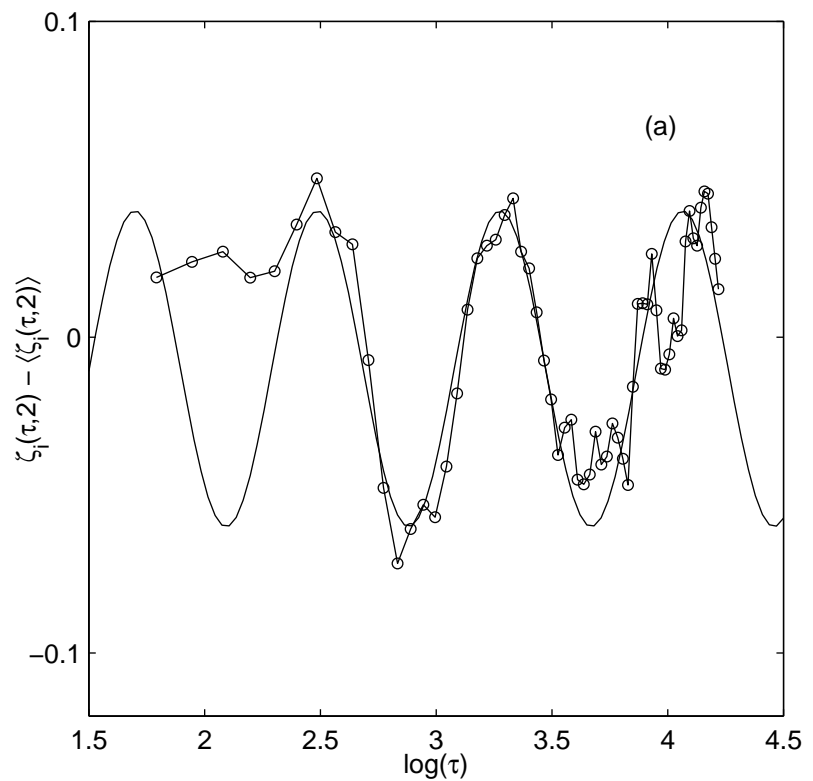


FIG. 2

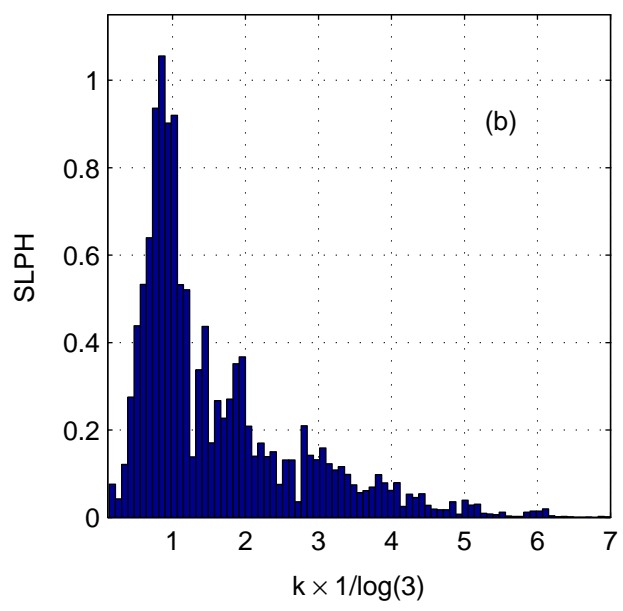
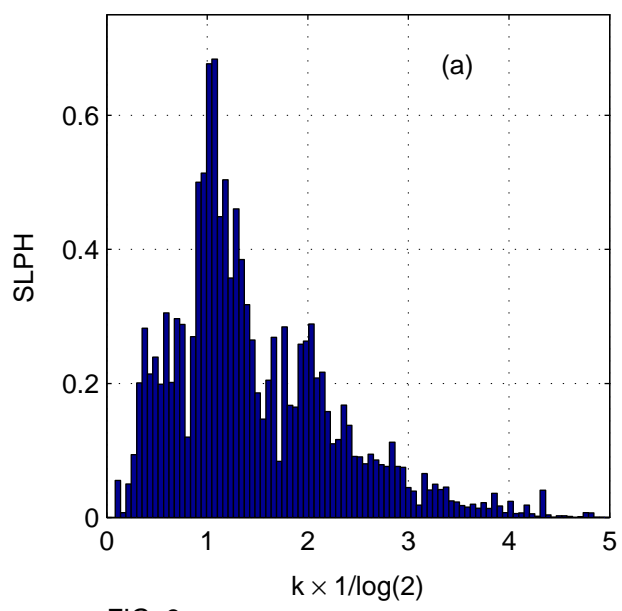


FIG. 3

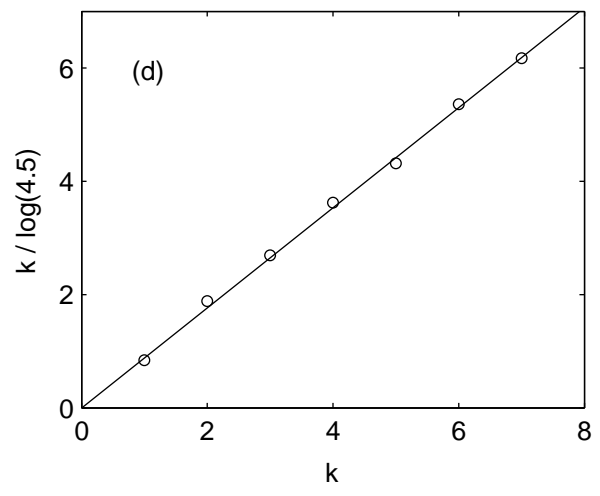
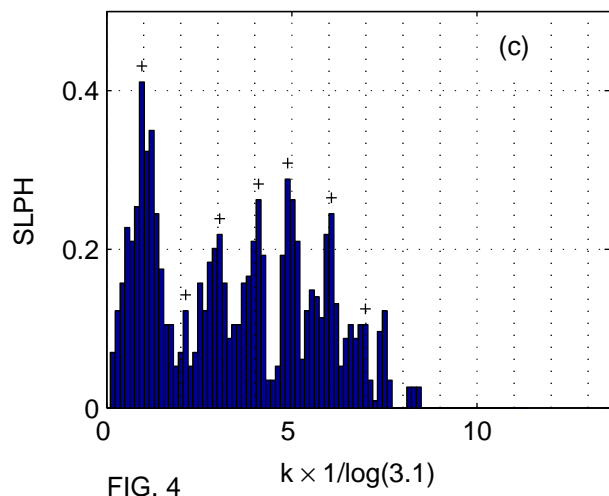
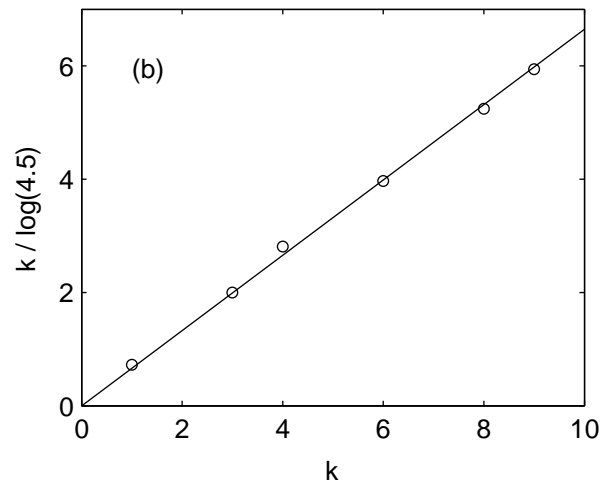
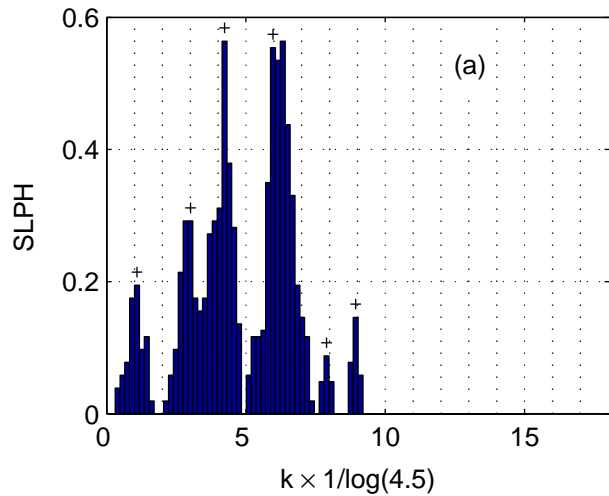


FIG. 4

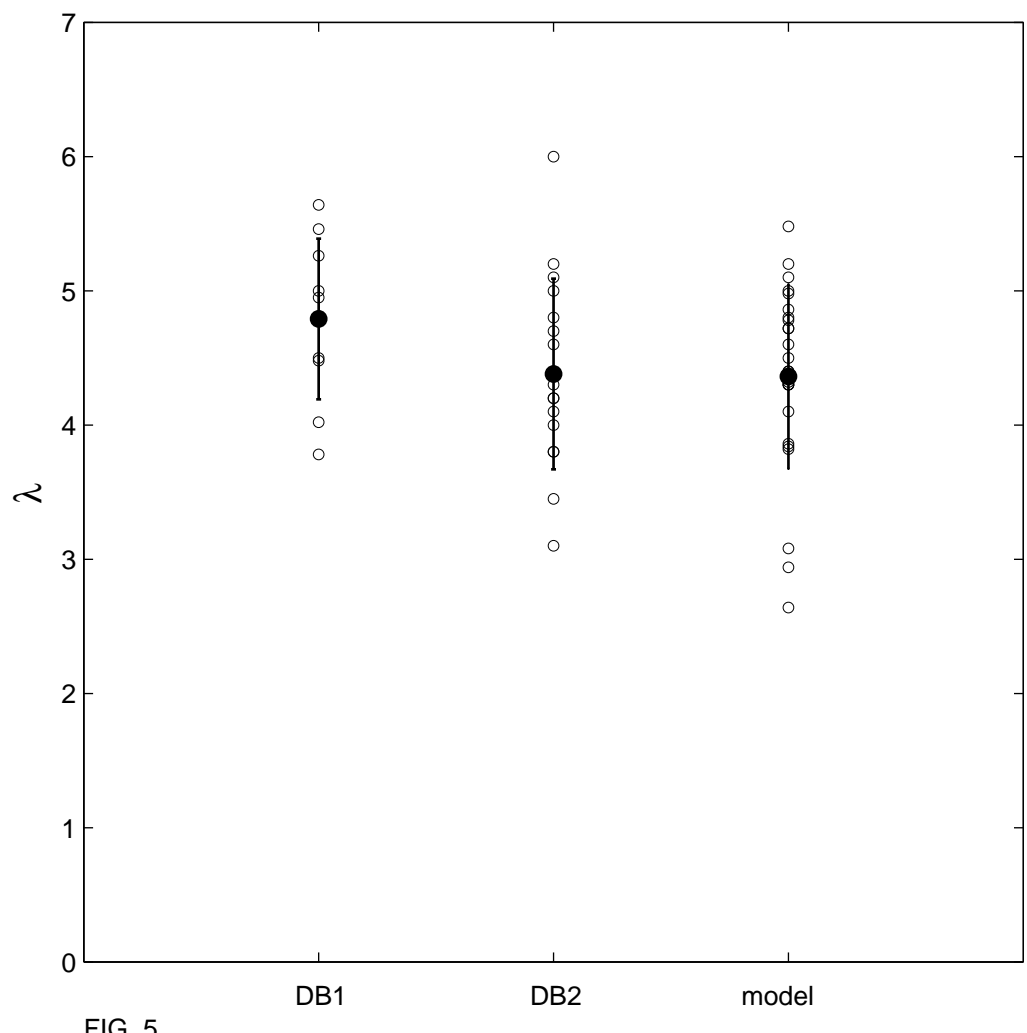
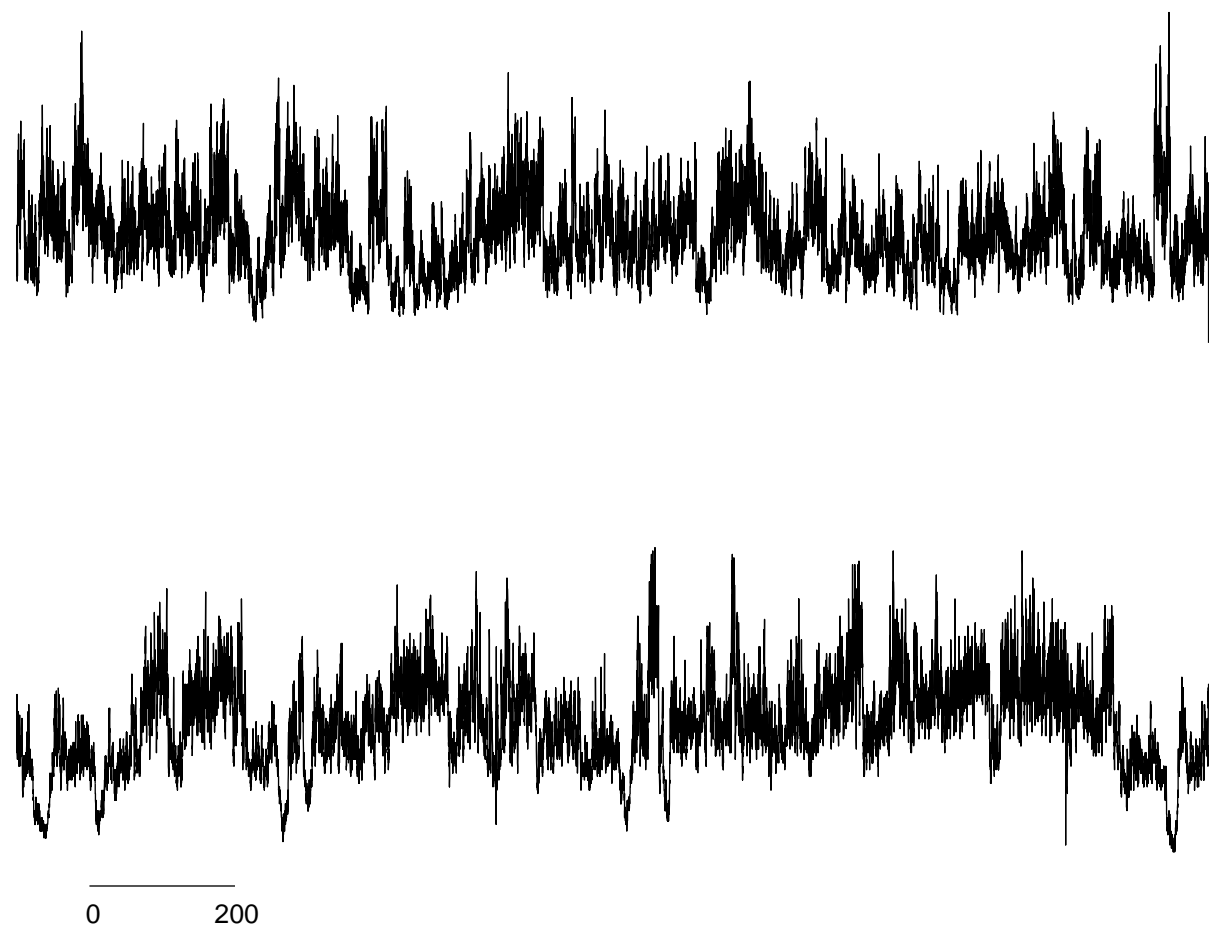


FIG. 5

FIG. 6



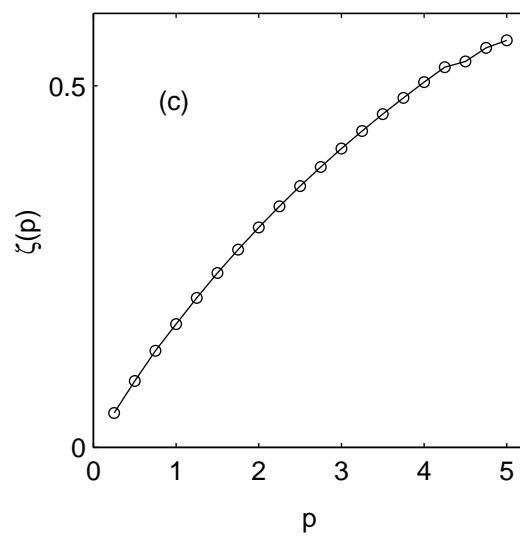
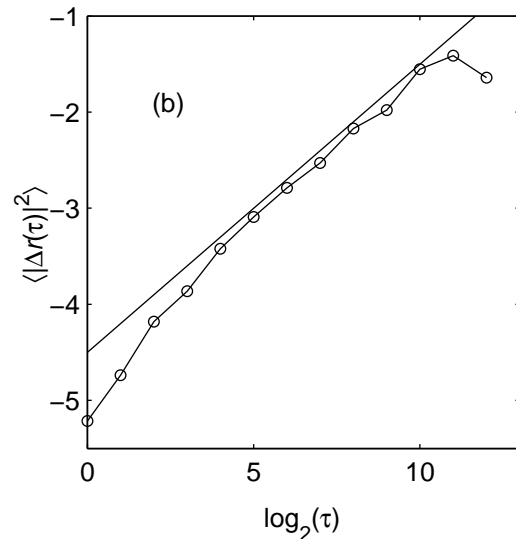
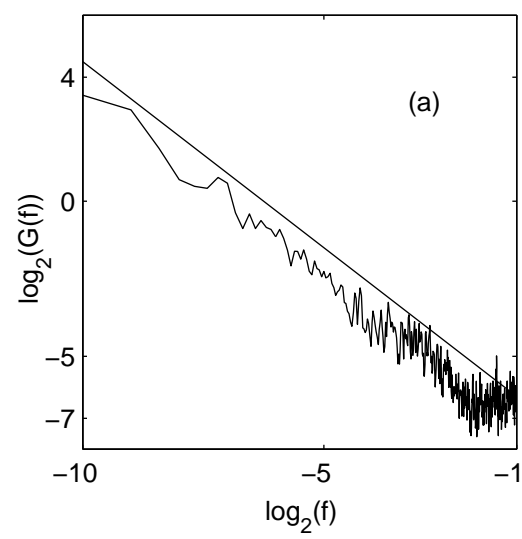


FIG. 7

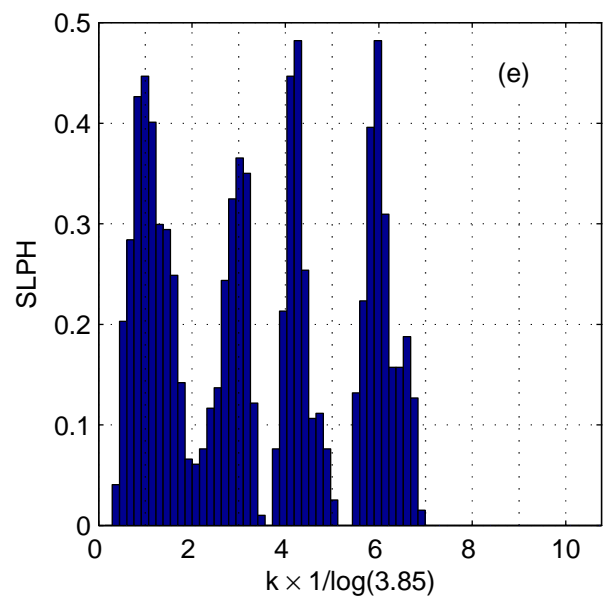
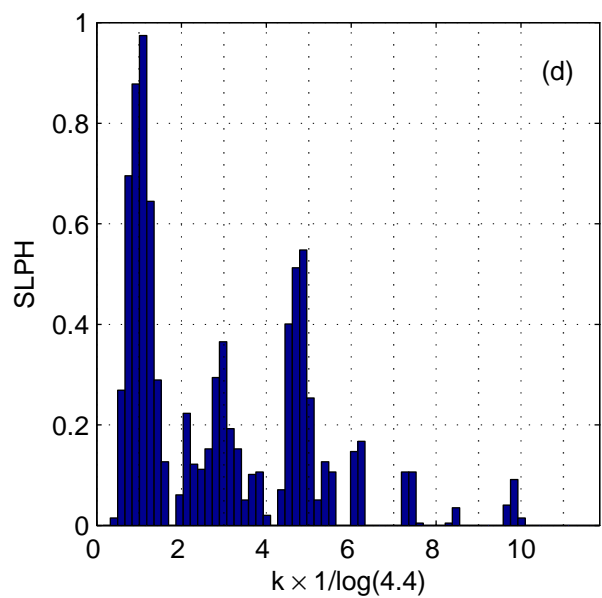


FIG. 7 (cont')